Synthesis and optical properties of environmentally benign and highly uniform $NaCe(MoO_4)_2$ based yellow nanopigments

Mariano Laguna, Nuria O. Núñez, Marcial Fernández and Manuel Ocaña*

Instituto de Ciencia de Materiales de Sevilla, CSIC, Américo Vespucio 49, 41092, Isla de la Cartuja, Sevilla, Spain

* corresponding author: mjurado@icmse.csic.es

Abstract

A method for the synthesis of uniform and aggregation free $NaCeMoO_4$ based nanospheroids with tunable size is reported. The procedure is based on a precipitation reaction at 120ºC for 20 h from solutions containing Na_2MoO_4, sodium citrate and $Ce(NO_3)_3$ and different amounts of $Y(NO_3)_3$ or $Gd(NO_3)_3$. The role played by the later compounds on the formation of the particles and their morphological and structural characteristics is analyzed through the analysis of the mechanism of particle formation. The chromaticity coordinates of the obtained samples are also evaluated showing that the here reported nanoparticles constitute an ecofriendly alternative to more toxic commercial yellow pigments. The synthesized nanoparticles are also free of aggregation in water suspensions and might be suitable for injet-printing technologies.

Key words: rare earth alloys and compounds; precipitation; optical properties; light absorption and reflection; optical spectroscopy

1. Introduction

Inorganic pigments are widely used to impart color to different objects in different fields such as ceramics, paints, inks and cosmetic [1], to mention a few. For these uses, inorganic pigments must be chemically inert, must be insoluble and colloidally stable in the medium in which they are dispersed. Particle size is an important issue when dealing with the application of inorganic pigments since this factor affects the scattering coefficient of the particles and therefore, their optical characteristics (luster, transparency, lightness) [1]. The decrease in particle size also favored the colloidal stability of the pigment particles and increases surface coverage of the object to be colored, thus favoring their performance. Finally, pigments particles with size lying within the nanometer range are mandatory for some applications. This is the case of inject printing, the most recent decoration technique developed for decoration of ceramic materials, for which tints based on nanopigments are essential since large particles sizes give rise to some operation problems such as nozzle clogging and dispersions instability [2].

Other important concern in the inorganic pigments field is toxicity. Thus, many traditional pigments contain toxic metal cations which are not permitted by modern regulations. For example, except praseodymium yellow (Pr doped zirconium silicate), most of the commercially available yellow pigments contain Pb, Ni, Cd or Sb cations [3], which are not desirable because of the above reason. Consequently, the development of alternative pigments, which are environmentally benign, is being a research topic of high interest. In this context, several new yellow pigment have been proposed which include some rare earth (RE) based phases such as titanium doped cerium molybdate [4], titanium doped praseodymium molybdate [5], molybdenum doped cerium oxide [6] and sodium cerium mixed molybdate [7]. However, to the best of our knowledge, none of these materials has been synthesized in the form of uniform and well dispersed nanoparticles.

In this work, we report for the first time a procedure, based on a homogeneous precipitation reaction in ethylene glycol-water solutions, for the synthesis of highly uniform and well dispersed (in aqueous medium) nanoparticles of a sodium cerium molybdate ($NaCe(MoO_4)_2$) ecofriendly yellow pigments. These particles showed an ellipsoidal shape and their mean size could be tuned in the range from 249 to 105 nm (length) and 134 to 61 nm (width) by doping with different amounts of rare earth (Gd^{3+}, Y^{3+}) cations. In order to explain such behavior, the mechanism of particle formation is analyzed. Finally, the color of the pigments is evaluated as a function of their size and composition.

2. Experimental

2.1. Reagents

Cerium (III) nitrate hexahydrate ($Ce(NO_3)_3 \cdot 6H_2O$, Aldrich, 99%), gadolinium (III) nitrate hexahydrate ($Gd(NO_3)_3 \cdot 6H_2O$, Aldrich, 99.9%) and yttrium (III) nitrate hexahydrate ($Y(NO_3)_3 \cdot 6H_2O$, Aldrich, 99.8%) were selected as rare earth precursors and sodium molybdate (Na_2MoO_4, Aldrich, ≥98%) was used as molybdate source. Sodium citrate ($Na_3C_6O_7H_5.2H_2O$, Aldrich, 99.5%) was also needed as complexing agent whereas ethylene glycol (EG, Aldrich, ≥99.5%)-water (Milli-Q) mixtures were used as solvent.

2.2. Synthesis of $NaCe(MoO_4)_2$ nanoparticles

The procedure for the synthesis of $NaCe(MoO_4)_2$ based nanoparticles was as follows: 0.25 mmol of $Ce(NO_3)_3$ and 0.5 mmol of sodium citrate were dissolved in 1 cm^3 of Milli-Q water and then 1.5 cm^3 of EG were added to this aqueous solution. In a separate vial, 0.5 mmol of Na_2MoO_4 were dissolved in 2.5 cm^3 of EG under magnetic stirring while heating the vial at ~80ºC to facilitate the dissolution process. The resulting solution (Ce concentration = 0.05 mol dm^{-3}, EG/water ratio by vol. = 4/1) was left to cool down to room temperature. The latter was then added to the solution containing the Ce precursor,

under magnetic stirring, and the mixture was quickly introduced in tightly closed test tubes and heated in an oven at 120 ºC in which, it was finally aged for 20 h. After aging, the resulting dispersions were cooled down to room temperature, centrifuged to remove the supernatants, the precipitates washed, twice with ethanol and once with double distilled water and finally dispersed in Milli-Q water. For some analyses, the powders were dried at room temperature.

2.3. Synthesis of RE-doped $NaCe(MoO_4)_2$ nanoparticles (RE= Y, Gd).

For the synthesis of RE-doped $NaCe(MoO_4)_2$ nanoparticles, we proceeded as described above for the case of the undoped system but incorporating the desired amount of Y or Gd to the starting $Ce(NO_3)_3$ solution. The total concentration of rare-earth cations was always kept constant (0.05 mol dm^{-3}).

2.4. Characterization

Particle shape was examined by transmission (TEM, Philips 200CM) and scanning (FEGSEM, Hitachi S4800, 20kV) electron microscopy. For this, a droplet of an aqueous suspension of the sample was deposited on a copper grid coated with a transparent polymer and dried. Particle size was measured by counting several hundred of particles from the TEM micrographs, as well as, by dynamic light scattering (DLS) measurements conducted in a Zetasizer NanoZS90 (Malvern) apparatus, which was also used for Z potential measurements.

The quantitative composition of the samples was analyzed by inductively coupled plasma atomic emission spectroscopy (ICP-AES, Horiba Jobin Yvon, Ultima 2). The infrared spectra (FTIR) of the nanoparticles diluted in KBr pellets were recorded in a Jasco FT/IR-6200 Fourier transform spectrometer.

The crystalline structure of the prepared particles was identified by X-ray diffraction (XRD, Panalytical X´Pert Pro with an X-Celerator detector). The unit cell parameters

were determined from the XRD data (collected at intervals of 0.02° (2θ) for an accumulated time of 1000 s) by Rietveld refinement using the X'Pert High Score Plus software. The structural data for the $NaCe(MoO_4)_2$ phase were taken from Teller [8]. The refined parameters were: zero, background coefficients, scale factor and lattice parameters. The obtained Rwp values were in all cases in the 10–14% range. The crystallite size was estimated from the most intense XRD peak of the $NaCe(MoO_4)_2$ (112) (2θ at 28.2º) by using the Scherrer formula.

To gain additional information on the morphological structural and compositional (elemental distributions within the particles), they were also characterized by High Angle Annular Dark Field Scanning TEM (HAADF-STEM) and High Resolution TEM by using a FEI Tecnai field emission gun STEM microscope (G2F30) working at 300 kV (0.2 nm point resolution) and equipped with a HAADF detector from Fischione (0.16 nm point resolution in STEM-HAADF mode) and an EDX detector SSD (INCA X-Max 80). EDX line profile spectra were recorded in STEM mode using a probe with a size of less than 1 nm. The HREM images and EDX spectra were processed using Gatan Digital Micrograph software. The Digital Diffraction Patterns (DDP) were obtained from the HRTEM images using the Tecnai Imaging and Analysis (TIA) software.

UV-visible diffuse reflectance spectra were recorded using a PerkinElmer UV-vis-NIR spectrometer (model Lambda 750S) equipped with an integrating sphere. Reflectance was converted to absorbance using the Kubelka-Munk equation.[1]

The color of the pigment was evaluated according to the Commission Internationale de l'Eclairage (CIE) through L*a*b* parameters [9]. In this system, L* is the color lightness (L*=0 for black and L*=100 for white), a* is the green (−)/red (+) axis, and b* is the blue (−)/yellow (+) axis. These parameters were measured (illuminant D65, standard observer

10°) using a Dr. Lange colorimeter (Model LUCI 100) and a white ceramic title (chromaticity coordinates: x=0.315, y=0.335) as the standard reference.

3. Results and discussion

3.1. Nanoparticles synthesis and characterization

One of the most common methods for the formation of uniform particles in solution is homogeneous precipitation. Such process requires a similar precipitation kinetics throughout the solution, which can be reached through a controlled release of anions or cations into the precipitating media [10]. To attain such conditions, in our case, we have used a Ce^{3+} precursor consisting of a Ln^{3+}–Cit^{3-} complex formed in the initial solution, which can be thermally decomposed at moderated temperatures thus liberating the Ce^{3+} cations involved in the formation of the solid phase, in a controlled manner [11]. This strategy has been adapted from that recently developed by us for the successful synthesis of uniform $NaGd(MoO_4)_2$ nanoparticles [12]. At first, we used the same experimental conditions (reagents concentration: Na_2MoO_4 (0.1 mol dm^{-3}), $Ce(NO_3)_3$ (0.05 mol dm^{-3}) and sodium citrate (0.1 mol dm^{-3}), temperature: 120ºC, solvent nature: ethylene glycol/water = 4/1, and aging time = 20 h) optimized for the Gd system. However, although under these conditions, the synthesized nanoparticles for the cerium case showed a homogeneous morphology (spheroidal), their size was heterogeneous (longest dimension between 60 and 190 nm) (Fig. 1a). It must be mentioned that the ethylene glycol/water ratio in the solvent mixture and the citrate concentration were found to be critical factors to obtain particles with homogeneous shape. Thus, when pure EG was used, no precipitation was detected, whereas for a EG/water ratio of 3/2, particles with irregular shape were formed. Finally, for a higher citrate concentration (0.25 mol dm^{-3}) no precipitation took place, whereas for a lower citrate concentration (0.05 mol dm^{-3}) the

solution precipitated immediately after adding the molybdate containing solution also yielding irregular particles.

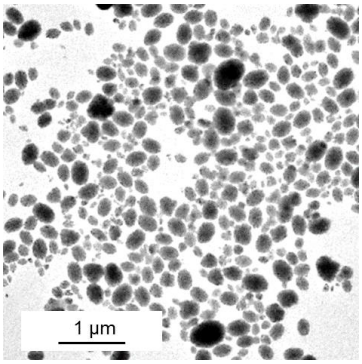

Figure 1. TEM image of the particles obtained by aging at 120ºC for 20 hours, a solution in ethylene glycol/water (4/1 by vol.) containing Na_2MoO_4 (0.1 mol dm^{-3}), $Ce(NO_3)_3$ (0.05 mol dm^{-3}) and sodium citrate (0.1 mol dm^{-3}).

Interesting, it was found that the addition of other RE (RE = Y^{3+} or Gd^{3+}) cations (nominal RE/RE+Ce mol ratio = 30%) to the precipitating solution had an important effect on the size distribution of the synthesized nanoparticles, which kept the spheroidal shape. Thus, homogeneous particles with a mean size of 161 x 94 nm, for Y (Fig. 2a), and 249 x 134 nm for Gd (Fig. 2d) doping, were obtained (Table 1).

Table 1. Shape, size (from TEM), hydrodynamic diameter (from DLS) and Z potential measured for the particles obtained from solutions containing Na_2MoO_4, $Ce(NO_3)_3$ and sodium citrate under the conditions described in the legend for Fig. 1 and in the presence of different amounts of Y^{3+} and Gd^{3+}. Standard deviations corresponding to the size distribution obtained from TEM pictures are shown in parentheses

RE/RE+Ce mole ratio Nominal (%)	Shape	Larger dimension (nm)	Shorter dimension (nm)	Hydrodynamic diameter (nm)	Z potential (mV)
30% Y	Spheroids	161 (15)	94 (9)	153	-35.4
50% Y	Spheroids	127 (15)	75 (11)	134	-33.7
70% Y	Spheroids	109 (13)	72 (7)	124	-34.8
30% Gd	Spheroids	249 (28)	134 (12)	224	-36.1
50% Gd	Spheroids	179 (16)	107 (9)	209	-35.5
70% Gd	Spheroids	105 (12)	61 (7)	103	-37.2

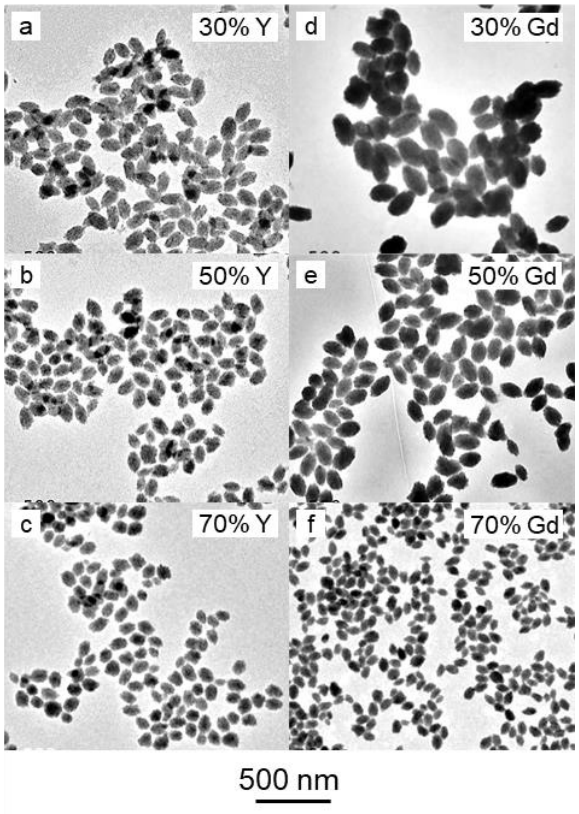

Figure 2. TEM images of the particles obtained by aging at 120ºC for 20 hours, a solution in ethylene glycol/water (4/1 by vol.) containing Na_2MoO_4 (0.1 mol dm^{-3}), sodium citrate (0.1 mol dm^{-3}) and $RE(NO_3)_3$ (0.05 mol dm^{-3}): RE: a) 70% Ce^{3+} and 30% Y^{3+}, b) 50% Ce^{3+} and 50% Y^{3+}, c) 30% Ce^{3+} and 70% Y^{3+}, d) 70% Ce^{3+} and 30% Gd^{3+}, e) 50% Ce^{3+} and 50% Gd^{3+}, f) 30% Ce^{3+} and 70% Gd^{3+}.

A further increase of the RE/RE+Ce mol ratio from 30 to 70% gave rise to a progressive decrease of particle size from 161x94 nm to 109x72 nm, in the case of Y addition, and from 249x134 nm to 105x61 nm in the case of Gd addition, while keeping a high

uniformity. Size variations on rare earths cations doping have been reported in recent works for different rare earth based systems synthesized by precipitation [13] and attributed to changes of the nucleation energy induced by the dopant cation, which modifies the number of nuclei formed thus changing the size that they will reach at the end of the growth stage [13].

The values of hydrodynamic diameter obtained from DLS measurement carried out for aqueous suspensions (pH = 6.5) of such nanoparticles (Fig. 3) were similar to the size determined from the TEM micrographs, indicating that the particles were highly dispersed. This behavior may be due to the high value of the zeta potential (between -34 and -37 mV) obtained for such dispersions, which involves a high repulsive interaction between the colloidal nanoparticles resulting in a high colloidal stability.

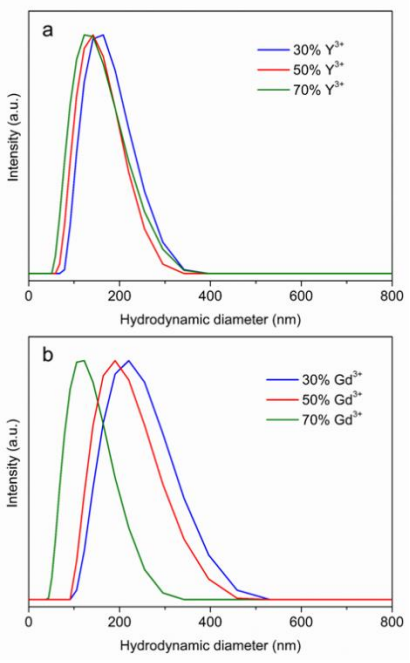

Figure 3. Size (hydrodynamic diameter) distribution obtained from DLS measurements carried out for aqueous dispersions at pH = 6.5 for the $NaCe(MoO_4)_2$ particles obtained in the presence of different amounts of: a) Y^{3+} and b) Gd^{3+}.

FTIR analyses gave information on the composition of the doped nanoparticles. Thus, the spectra recorded for the particles obtained in the absence or the presence of 50% Y^{3+} or

50% Gd^{3+} cations (Fig. 4) displayed the bands characteristics of the MoO_4^{2-} lattice vibrations (< 1000 cm^{-1}) [7] along with two broad features centered at 3400 and 1580 cm^{-1} due to absorbed water. Some additional bands in the 3100-2800 and the 1600-1400 cm^{-1} regions were also detected, which must be attributed to vibration modes of C-H and carboxylate groups, respectively, coming from citrate anions adsorbed on the nanoparticles surface [14]. These anions may act as capping agents controlling particle growth and might also contribute to the higher colloidal stability of the obtained nanoparticles due to their well-known dispersing ability.

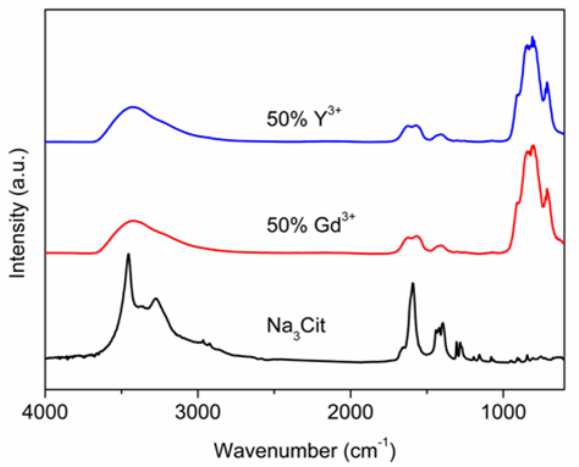

Figure 4. FTIR spectra obtained for the particles obtained in the absence and the presence of 50% Y^{3+} and 50% Gd^{3+}. The sodium citrate spectrum is also included.

XRD diffraction (Fig. 5) indicated that all nanoparticles obtained either in the absence or the presence of Y or Gd cations crystallized into the tetragonal $NaCe(MoO_4)_2$ phase.

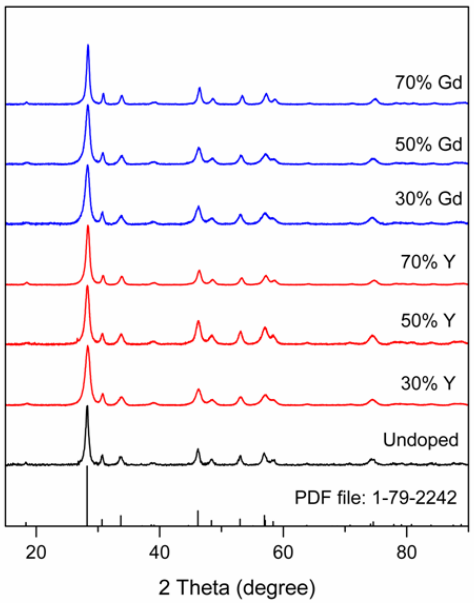

Figure 5. X-ray diffraction patterns for the particles obtained in the absence and the presence of different amounts of Y^{3+} and Gd^{3+}. The PDF file for tetragonal $NaCe(MoO_4)_2$ is also included.

The values of crystallite size obtained from these patterns (Table 2) were in all cases much smaller (from 20 to 40 nm) than the size of the particles indicating that they were polycrystalline, as confirmed by the DDP obtained from a HRTEM image of a single nanoparticle. This is illustrated in figure 6, which corresponds to the sample obtained by addition of a 70% of Gd. As observed in the inset of figure 6a, the DDP obtained for the whole particle shows elongated spots suggesting the presence of crystallites that are slightly misoriented. These data suggests that the spheroidal nanoparticles are formed by an ordered aggregation of smaller subunits as is the case of many previously reported RE based nanoparticles [15-17].

Table 2. Composition (RE/RE+Ce mole ratio) as determined from ICP and the Vegard´s law, unit cell parameters, unit cell volume and crystallite size measured for the particles obtained from solutions containing Na_2MoO_4, $Ce(NO_3)_3$ and sodium citrate under the conditions described in the legend for Fig. 1 and in the presence of different amounts of Y^{3+} and Gd^{3+}.

RE/RE+Ce mole ratio Nominal (%)	RE/RE+Ce mole ratio ICP (%)	RE/RE+Ce mole ratio Vegard´s law (%)	a=b (Å)	c (Å)	Cell volume (Å^3)	Crystallite size (nm)
0 %			5.3251 (6)	11.675 (2)	331.068	39
30% Y	1.71% Y	1.68% Y	5.3251 (6)	11.673 (2)	330.651	18
50% Y	6.50% Y	6.42% Y	5.3210 (1)	11.663 (3)	329.472	19
70% Y	16.23% Y	15.9% Y	5.3084 (4)	11.630 (1)	327.111	21
30% Gd	4.38% Gd	4.48% Gd	5.3215 (7)	11.663 (2)	330.285	22
50% Gd	11.92% Gd	11.5% Gd	5.3161 (5)	11.644 (2)	329.070	31
70% Gd	30.85% Gd	29.8% Gd	5.3010 (4)	11.597 (1)	325.888	37

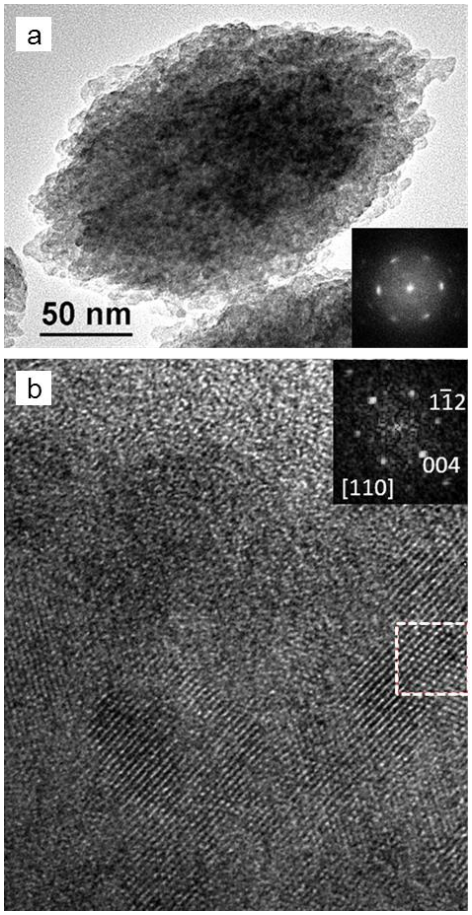

Figure 6. (a) HRTEM image of a nanoparticle corresponding to the sample doped with a 70% Gd and its corresponding DDP, (b) HRTEM detail and indexed DDP obtained from the marked area.

The DDP (Fig. 6b, inset) obtained for a single domain (white square in Figure 6b), in which the spots assigned to the (1-12) and (004) planes of the tetragonal $NaCe(MoO_4)_2$ phase were detected, corresponds to the [110] zone axis of such structure.

The unit cell parameters estimated from the XRD diffraction patterns were found to decrease as RE dopant concentration increased (Table 2) indicating the incorporation of the doping cations into the $NaCe(MoO_4)_2$ structure on the basis of the smaller ionic radii of Y^{3+} (1.019 Å) and Gd^{3+} (1.053 Å) when compared with that of Ce^{3+} (1.143 Å). It was surprising that although the radius of Gd^{3+} is higher than that of Y^{3+}, the cell volume of the Gd-doped samples was slightly smaller than that of the Y-doped ones (Table 2). To explain this behavior, the unit cell volume expected for the doped samples according to the Vegard´s law were calculated and plotted along with the experimental values vs. the nominal RE/RE+Ce mol ratio (Fig. 7).

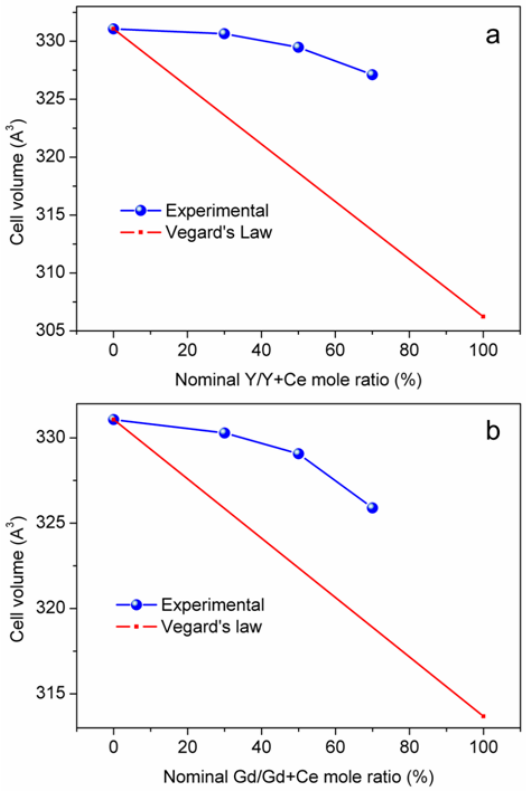

Figure 7. Experimental and calculated, according to the Vegard´s law, unit cell volume for the RE-doped samples having different doping levels

It was first observed that in all cases the theoretical values were smaller than those experimentally obtained indicating that the amount of doping cations incorporated to the $NaCe(MoO_4)_2$ structure was smaller than the nominal value, which was confirmed by ICP measurements (Table 2). Incidentally, the RE/RE+Ce mol ratio values obtained from ICP were in close agreement with those calculated from the Vegard´s law for all samples (Table 2). It was also noticed that the Gd incorporation was more effective than that of Y (Table 2) thus explaining the lower unit cell volume of the Gd-doped samples when compared to the Y-doped ones. These findings suggest that the kinetic of Gd and Y precipitation is slower than that of Ce as further confirmed by following the evolution of the precipitates with aging time. As illustrated for the Gd case, spheroidal particles were already formed after 3 h of aging whose size gradually increased from 34 x 21 nm to their final size (105 x 61 nm) on further heating up to 20 h (Fig. S1), with no changes in crystalline structure, which always corresponded to the $NaCe(MoO_4)_2$ tetragonal phase (Fig. S2). More interesting, the unit cell volume (Table 3) was found to decrease also gradually with aging time indicating a progressive Gd^{3+} incorporation to the formed particles (Fig. 8) and therefore, that the kinetic of Ce^{3+} precipitation is faster than that of Gd^{3+}, under the here used experimental conditions.

Table 3. Size, unit cell parameters, unit cell volume and composition (RE/RE+Ce mole ratio) as determined from the Vegard´s law for the particles obtained by aging for different periods of time solutions containing Na_2MoO_4, $Ce(NO_3)_3$ and sodium citrate under the conditions described in the legend for Fig. 1 and in the presence of 70% Gd^{3+}.

Reaction time (h)	**Larger dimension (nm)**	**Shorter dimension (nm)**	**a=b (Å)**	**c (Å)**	**Cell volume ($Å^3$)**	**Gd/Gd+Ce mole ratio (%)**
3	34 (5)	21 (4)	5.3173(8)	11.633(2)	328.910	12.41
6	67 (8)	36 (6)	5.3120(10)	11.632(3)	328.190	16.55
9	73 (8)	43 (5)	5.3058(4)	11.619(1)	327.093	22.87
15	97 (11)	56 (5)	5.3016(4)	11.607(1)	326.229	27.83
20	105 (12)	61 (7)	5.2993(3)	11.595(1)	325.613	30.85

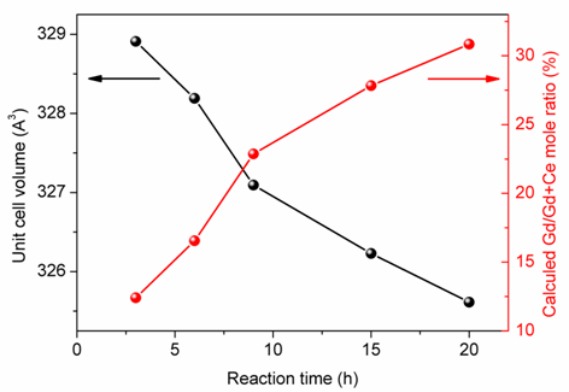

Figure 8. Unit cell volume and Gd content calculated according to the Vegard´s law for the $NaCe(MoO_4)_2$ samples doped with a 70% (nominal) Gd, as a function of aging time.

In agreement with such interpretation is the EDX profile (Fig. 9b) obtained along the marked line in the HAAF-STEM image of a nanoparticle shown in figure 9a. As observed, whereas the Ce, Mo and Na contents follows the particle geometry (i.e. such content is higher in the center of the particle in which the thickness is higher), the Gd content is almost constant all along the line indicating an enrichment of Gd in the particle outer layers.

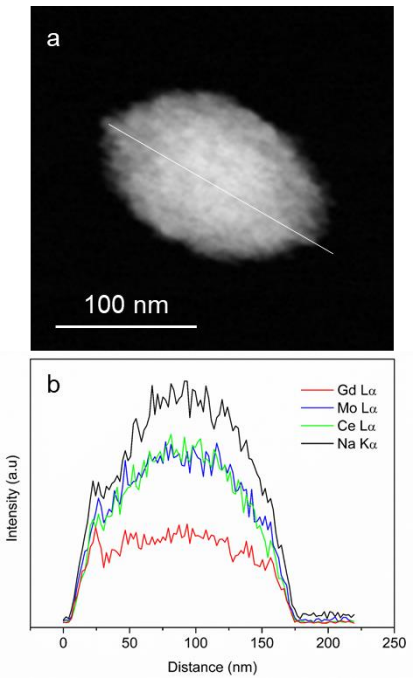

Figure 9. (a) HAAF-STEM image of a nanoparticle corresponding to the sample doped with a 70% (nominal) Gd. (b) EDX line profile along the marked line in (a).

3.2. Optical properties

The visible reflectance and absorption spectra measured for the RE-doped samples are shown in Figure 10. As observed, all spectra display a broad adsorption band starting at about 580 nm and centered at about 400 nm. Such an absorption in the blue region could be attributed to an O_{2p}-Ce_{4f} charge transfer transition, following a previous report on Mo-doped cerium oxide based pigments [6], and is responsible for the yellow color observed for the samples (Fig. 10, inset).

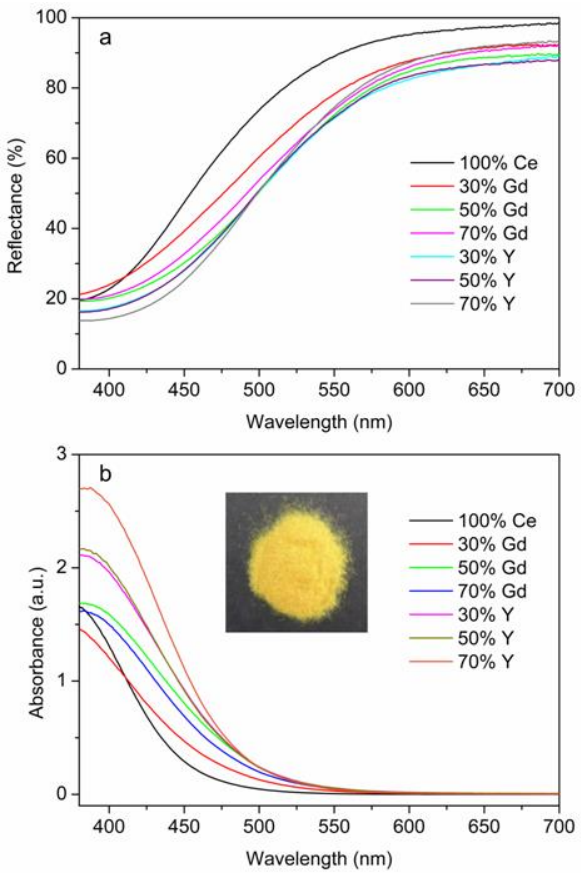

Figure 10. UV-visible reflectance (a) and absorbance (b) spectra for the RE-doped samples. Inset: Photograph of the pigment powder obtained by doping with a 70% (nominal) Gd.

The chromaticity coordinates in the L*a*b* color space measured for all uniform doped samples are shown in Table 4. As observed, the values for the b* component were always >30, in agreement with the yellow color indicated by the reflectance measurements. The a* values were between about 5 and 12 indicating a slight orange hue, which was higher

for the Gd doped samples. Finally, the lightness (L*) was similar for all samples (70 ± 2) indicating a similar color intensity.

Table 4. L*a*b* parameters for the RE-doped $NaCe(MoO_4)_2$ pigments

RE/RE+Ce mole ratio Nominal (%)	L*	a*	b*
30% Y	70.8	5.9	30.7
50% Y	71.3	6.2	41.9
70% Y	70.8	5.8	37.6
30% Gd	68.7	9.4	40.8
50% Gd	67.9	9.5	33.4
70% Gd	70.2	12.2	39.4

Conclusions

Uniform $NaCeMoO_4$ based nanospheroids can be obtained by a precipitation reaction at 120ºC for 20 h from solutions containing Na_2MoO_4, sodium citrate and $Ce(NO_3)_3$ and different amounts of $Y(NO_3)_3$ or $Gd(NO_3)_3$ as dopant. The addition of the later compounds is essential to achieve homogeneous size in the nanometer range. This synthesis method allows tuning particle size by changing the Y or Gd doping level. The obtained nanoparticles crystallized into the tetragonal $NaCeMoO_4$ structure and were composed by smaller crystallites slightly missoriented, indicating that they were formed through an ordered aggregation process. Irrespective of the doping cation or doping level, all obtained nanoparticles showed a yellow color with a slight orange hue which was higher for the Gd-doped pigments. These pigments constitute an ecofriendly alternative to more toxic commercial pigments. The synthesized nanoparticles are also free of aggregation in water suspensions and might be suitable for injet-printing technologies.

Acknowledgements

This work has been supported by the Spanish Ministry of Economy and competitiveness (MINECO) (MAT2014-54852-R) and CSIC (PIE 201460E005). We also thank Dr. Cristina Rojas and Dr. Jorge Gil for their assistance in obtaining HRTEM and diffuse reflectance data, respectively.

References

[1] Buxbaum G, Pfaff G. Industrial Inorganic Pigments. 3rd ed. Weinheim: Wiley-VCH Verlag GmbH; 2005.

[2] Cavalcante PMT, Dondi M, Guarini G, Raimondo M, Baldi G. Colour performance of ceramic nano-pigments. Dyes Pigm 2009;80:226–32.

[3] Classification and chemical description of the complex inorganic colour pigments. Alexandria, VA: Dry Color Manufacturer`s Association; 1991.

[4] Furukawa S, Masui T, Imanaka N. Synthesis of new environment-friendly yellow pigments. J Alloys Comp 2006;418:255–8.

[5] George G. The structural and optical studies of titanium doped rare earth pigments and coloring applications. Dyes Pigm 2015;112:81–5.

[6] Radhika SP, Sreeram KJ, Nair BU. Mo-doped cerium gadolinium oxide as environmentally sustainable yellow pigments. ACS Sustainable Chem Eng 2014;2:1251–6.

[7] Sreeram KJ, Srinivasan R, Devi JM, Nair BU, Ramasami T. Cerium molybdenum oxides for environmentally benign pigments. Dyes Pigm 2007;75:687–92.

[8] Teller RG. Refinement of some $Na_{0.5-x}M'_{0.5-x/3}\square_{2x/3}MoO_4$, *M* = Bi, Ce, La, Scheelite Structures with Powder Neutron and X-ray Diffraction Data. Acta Crystallogr, Sect C: Cryst Struct Commun 1992;48:2101–4.

[9] Commission Internationale de l'Eclairage Recommendations on Uniform Colour Spaces, Colour Difference Equations, Psychometrics Colour Terms, Supplement no. 2 of CIE Publication no.15 (E1-1,31) 1971. Bureau Central de la CIE, Paris, 1978.

[10] Matijevic E. Preparation and properties of uniform size colloids. Chem Mater 1993;5:412–26.

[11] Wang H, Wang L. One-pot synthesis and cell imaging applications of Poly(amino acid) coated $LaVO_4:Eu^{3+}$ luminescent nanocrystals. Inorg Chem 2013;52:2439–45.

[12] Laguna M, Nuñez NO, Rodríguez V, Cantelar E, Stepien G, García ML et al. Multifunctional Eu-doped $NaGd(MoO_4)_2$ nanoparticles functionalized with poly(L-lysine) for optical and MRI imaging. Dalton Trans 2016;45:16354–65.

[13] Chen D, Wang Y. Impurity doping: a novel strategy for controllable synthesis of functional lanthanide nanomaterials. Nanoscale 2013;5:4621–37.

[14] Zhao J, Sun Y, Kong X, Tian L, Wang Y, Tu L. Controlled synthesis, formation mechanism and great enhacement of red upconversion luminescence of $NaYF_4:Yb^{3+},Er^{3+}$ nanocrystals/submicroplates at low doping level. J Phys Chem B 2008;112:15666–72.

[15] González-Mancebo D, Becerro AI, Rojas TC, García-Martín ML, de la Fuente JM, Ocaña M. HoF_3 and DyF_3 nanoparticles as contrast agents for high-field magnetic resonance imaging. Part Part Syst Charact 2017:1700119–25.

[16] Becerro AI, González-Mancebo D, Ocaña M. Uniform, luminescent $Eu:LuF_3$ nanoparticles. J Nanopart Res 2015;17:58.

[17] Laguna M, Nuñez NO, Becerro AI, Ocaña M. Morphology control of uniform $CaMoO_4$ microarchitectures and development of white light emitting phosphors by Ln doping (Ln = Dy^{3+}, Eu^{3+}). CrystEngComm 2017;19:1590–1600.